On-Chip Andreev Devices: Hard Superconducting Gap and Quantum Transport in Ballistic Nb–In$_{0.75}$Ga$_{0.25}$As-Quantum-Well–Nb Josephson Junctions

Kaveh Delfanazari,* Reuben K. Puddy, Pengcheng Ma, Teng Yi, Moda Cao, Yilmaz Gul, Ian Farrer, David A. Ritchie, Hannah J. Joyce, Michael J. Kelly, and Charles G. Smith

A superconducting hard gap in hybrid superconductor–semiconductor devices has been found to be necessary to access topological superconductivity that hosts Majorana modes (non-Abelian excitation). This requires the formation of homogeneous and barrier-free interfaces between the superconductor and semiconductor. Here, a new platform is reported for topological superconductivity based on hybrid Nb–In$_{0.75}$Ga$_{0.25}$As-quantum-well–Nb that results in hard superconducting gap detection in symmetric, planar, and ballistic Josephson junctions. It is shown that with careful etching, sputtered Nb films can make high-quality and transparent contacts to the In$_{0.75}$Ga$_{0.25}$As quantum well, and the differential resistance and critical current measurements of these devices are discussed as a function of temperature and magnetic field. It is demonstrated that proximity-induced superconductivity in the In$_{0.75}$Ga$_{0.25}$As-quantum-well 2D electron gas results in the detection of a hard gap in four out of seven junctions on a chip with critical current values of up to 0.2 µA and transmission probabilities of >0.96. The results, together with the large *g*-factor and Rashba spin–orbit coupling in In$_{0.75}$Ga$_{0.25}$As quantum wells, which indeed can be tuned by the indium composition, suggest that the Nb–In$_{0.75}$Ga$_{0.25}$As–Nb system can be an excellent candidate to achieve topological phase and to realize hybrid topological superconducting devices.

There has been renewed interest in hybrid superconducting–semiconducting–superconducting (S–Sm–S) junctions and Andreev devices[1] because of the recently reported detection of Majorana particles at the interfaces of these junctions (hybrid topological materials). As such, these structures have been proposed for the building blocks of the next generation of quantum computers.[2–4] However, there still is a fundamental technological problem in the fabrication of highly transparent interfaces between superconductors and semiconductors and scaling the number of junctions up in a single chip to realize a quantum device applicable for quantum technology. In this regard, there have so far been significant efforts in making high-quality S–Sm interfaces with transmission probability of almost unity. Most of the earlier reports showing the signature of a hard gap, and therefore the fabrication of highly transparent interfaces, are based on indium arsenide (InAs) in a 2D electron gas (2DEG) formed in a quantum well in a heterostructure or as a 1D nanowire. This work involved the in situ deposition of Al on InAs in a molecular beam epitaxy (MBE) chamber after the semiconductor growth has been completed.[5] This is believed to work because the interface is very clean and Al makes good contact to the InAs as the Fermi energy in InAs is pinned in the conduction band at the surface resulting in the formation of high-quality and transparent S–Sm interfaces. Similar high-quality interfaces were also reported in an inverted gallium arsenide (GaAs) heterojunction structures fabricated with niobium nitride (NbN) contacts.[6] However, in comparison with these materials, the low electron effective mass, large *g*-factor, and Rashba spin–orbit coupling in indium gallium arsenide (In$_x$Ga$_{1-x}$As)

Dr. K. Delfanazari, Dr. R. K. Puddy, P. Ma, T. Yi, M. Cao, Dr. I. Farrer,
Prof. D. A. Ritchie, Prof. M. J. Kelly, Prof. C. G. Smith
Department of Physics, Cavendish Laboratory
University of Cambridge
Cambridge CB3 0HE, UK
E-mail: kd398@cam.ac.uk
Dr. K. Delfanazari, Dr. H. J. Joyce, Prof. M. J. Kelly
Centre for Advanced Photonics and Electronics
Electrical Engineering Division
University of Cambridge
Cambridge CB3 0FA, UK

Y. Gul
Department of Electronic and Electrical Engineering
University College London
London WC1E 7JE, UK
Dr. I. Farrer
Department of Electronic and Electrical Engineering
University of Sheffield
Mappin Street, Sheffield S1 3JD, UK

quantum wells make InGaAs a very attractive material in the field of topological quantum computing, electronics, spintronics, and photonics.[7] In addition to all these advantages, the ability to tune the indium composition allows the formation of highly transmissive metal–semiconductor interfaces which we discuss in this paper. We study the fabrication and low-temperature measurements of eight symmetric S–Sm–S planar and ballistic Josephson junctions on a chip containing an $In_{0.75}Ga_{0.25}As$ quantum well in a heterostructure in which each junction consists of two identical niobium (Nb) superconducting electrodes in contact with a 2DEG that is formed ≈120 nm below the wafer's surface. Each junction is measured individually using a lock-in measurement technique. The measurements are carried out in a dilution fridge with a base temperature of 40 mK in a magnetic field of up to 9 T and the quantum transport of the junctions are measured below 800 mK. We observe large critical currents and a U-shape hard gap at low source–drain voltage bias V_{SD} due to Andreev bound states at the S–Sm interfaces in four out of seven working junctions while the other three show evidence of a soft gap. The subharmonic energy gap structures (SGS)[8] are observed when the applied V_{SD} satisfies the expression $V = 2\Delta/ne$, where the Δ is the Nb superconducting gap energy ($2\Delta_{Nb} \approx 2.2$ meV), $n = 1, 2, 3, ...$ is an integer, and e is the electron charge. The SGS are clearly observed that are strongly temperature and magnetic field dependent.

Results from the Experiments: **Figure 1**b shows a false color scanning electron microscopy (SEM) image of the on-chip Andreev device, consisting of eight symmetric and planar Nb–$In_{0.75}Ga_{0.25}As$–Nb Josephson junctions. In Figure 1c, the zoomed-in image of the junction 3 (J3) is shown and this junction will be discussed here in detail. All junctions are in the ballistic regime as the distance (shortest path where superconducting electrode's wave functions in each side could overlap) between the two Nb electrodes is 850 nm which is shorter than the corresponding elastic mean free path $\ell_e = e^{-1} \hbar \mu_e \sqrt{2\pi n_s} \approx 2$ μm.

The differential resistance dV/dI versus V_{SD} at 50 mK for four junctions with a hard superconducting gap are shown in **Figure 2**a. An excess current I_{exc} flows through the junctions as a result of electron- and hole-like quasiparticles correlations

(Andreev reflections) below the junction's T_c' and for voltage biases within the superconducting gap. The dV/dI (V_{SD}) value is reduced in the gap region and a U-shape dip which is a signature of a hard gap[5] is observed for junction numbers 2, 3, 5, and 7, where supercurrents with critical currents of up to 2 μA are measured. However, the results for junction numbers 1, 4, and 6 are different and they show a soft gap signature[9,10] in which the junction resistance drops but dV/dI (V_{SD}) is not flat. The origin of the soft gap is not fully understood, however, this has so far been explained by the effect of inhomogeneities at the S–Sm interfaces together with quasiparticle broadening.[9] In our junctions, this difference may be due to a residue altering the wet etching process resulting in a tunneling barrier at the interface or variation in the etch depth so that the Nb trench in which the Nb sits is not deep enough in some areas. In this case, the resulting tunneling barrier leads to a reduction of the excess current with both normal and Andreev reflections competing together. These devices will be discussed in detail elsewhere. We could not measure quantum transport, neither a hard- nor soft-gap structure for junction number 8 because of a wire contact failure between the device and pad.

Temperature Dependence of Induced Superconductivity in $In_{0.75}Ga_{0.25}As$: The dV/dI (V_{SD}) curves for temperatures between 50 and 800 mK for junction number 3 are plotted in Figure 2b where the curves are shifted vertically upward by 0.5 kΩ for clarity.

The current–voltage characteristics (IVC) of the junction is plotted in **Figure 3**a at various temperatures by integration of dV/dI (V_{SD}). A pronounced supercurrent and quantum transport between two Nb superconducting junctions are observed at zero magnetic field and at low temperatures between 50 and 500 mK. The largest critical current (I_c) was measured at the lowest temperature of 50 mK. As shown in Figure 3b for junctions 3 and 5, I_c is suppressed as the temperature increases and totally disappeared above 600 and 300 mK for these two junctions, respectively. This is due to the relatively large distance between the two Nb electrodes (850 nm) and the normal state resistance of the junctions ($R_N \approx 0.1$–0.8 kΩ). However, we observed a flat dV/dI (V_{SD}) within Δ/e which suggests
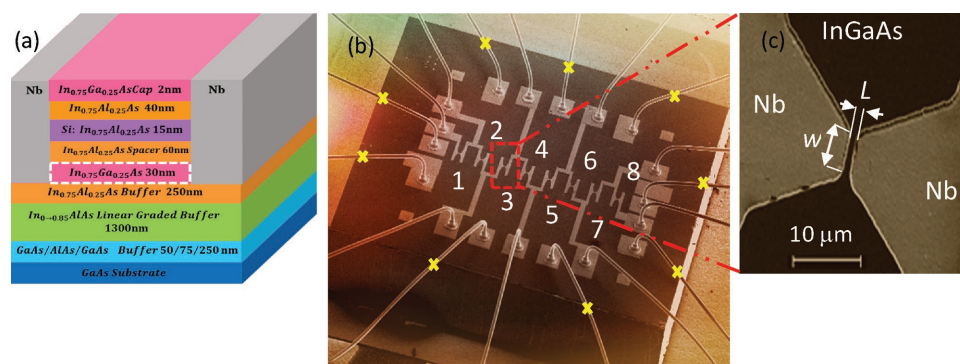

Figure 1. On-chip superconductor–semiconductor–superconductor ballistic Josephson junctions: a) The schematic view of the $In_{0.75}Ga_{0.25}As$/$In_{0.75}Al_{0.25}As$/GaAs heterostructure. Niobium (Nb) was used as the superconducting contacts (shown in gray) to form a hybrid Nb–$In_{0.75}Ga_{0.25}As$-2DEG–Nb Josephson junction. The $In_{0.75}Ga_{0.25}As$ quantum well is formed ≈120 nm below the wafer surface (shown in pink with white dashed rectangle). The active channel (mesa structure) is the region that is sandwiched between two Nb electrodes (see the second and third paragraphs). b) False color scanning electron micrograph (SEM) image of the device showing a top view of eight symmetric Josephson junctions on a chip. Those wires that were not used in this study are marked yellow. c) The zoomed-in image of junction 3 shown in (b). The gap between the two Nb electrodes has a length $L = 850$ nm and a width $w = 4$ μm.
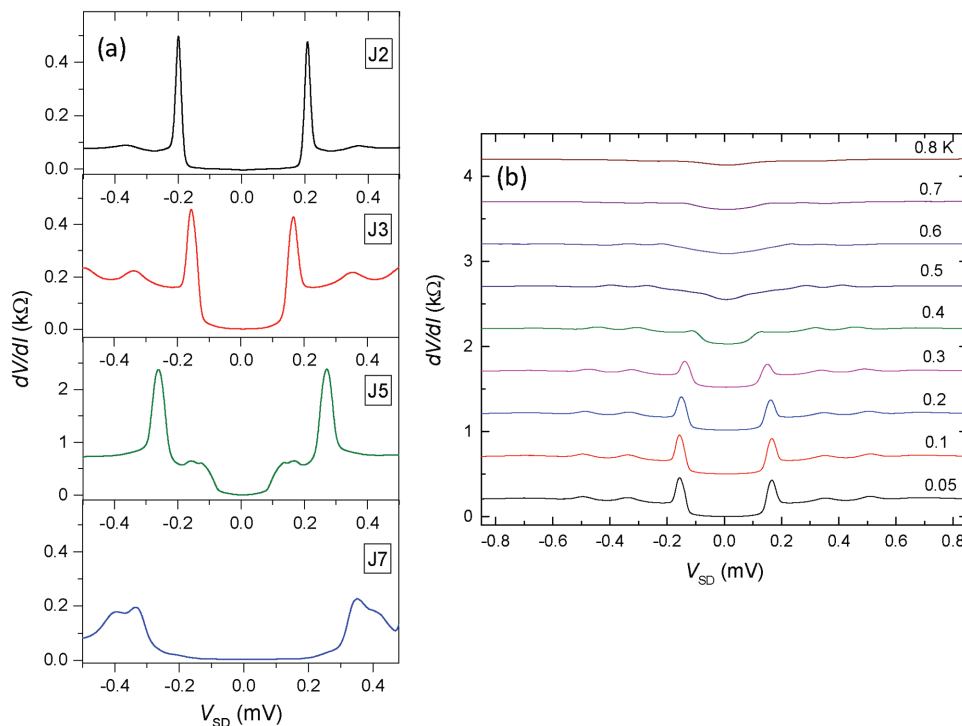
**ADVANCED
SCIENCE NEWS**

www.advancedsciencenews.com

**ADVANCED
MATERIALS**

www.advmat.de

Figure 2. Induced superconducting properties in an $In_{0.75}Ga_{0.25}As$ quantum well: a) Hard superconducting gap in dV/dI (V) curves measured in junction number 2, 3, 5, and 7, at temperature 50 mK. Differential resistance dV/dI versus source–drain voltage (V_{SD}) for junction 3 at temperatures between 50 and 800 mK. The curves are shifted vertically by 0.5 kΩ for clarity.

interface fabrication with high transparency based on Blonder–Tinkham–Klapwijk (BTK) theory.[11]

As shown in Figure 3c, the SGS structures correspond to $\Delta/2e$ (cyan dashed line), $\Delta/3e$ (light-green dashed line), and gap edge (light-pink dashed line) are observed for junction 3. The shape of the gap and SGS has been shown to be influenced by the ratio of L/ξ_N,[6,11–13] where ξ_N is the Bardeen–Cooper–Schrieffer coherence length. The SGS consists of a set of pronounced maxima in dV/dI at $V = 2\Delta/ne$ if $L/\xi_N \ll 1$, but the amplitude of the SGS decreases by increasing the ratio of L/ξ_N. For $L \approx \xi_N$ the peaks evolve into dips. To find the ratio between L and ξ_N in our junction we shall point out that in our chip the heterostructure has a quantum well with 30 nm thickness formed ≈120 nm below the wafer's surface and sandwiched between InAlAs layers. Using $\Delta_{Nb} = 1.1$ meV and the equation $\xi_N = \hbar v_{FN}/\pi\Delta_{Nb}$, the coherence length of the 2DEG is calculated as $\xi_N = 177$ nm. However, because of the proximity effect a minigap is induced into the 2DEG and the Δ_{Nb} will be replaced with a smaller value $\Delta_{ind} = 1.76$ $k_B T'_c \approx 100$ μeV which results in $\xi_N \approx 2$ μm.[6] Therefore we consider the junction with a hard gap to be a short ballistic junction ($L/\xi_N \ll 1$). Thus the flat dV/dI (V_{SD}) observed within Δ_{Nb} for four junctions are consistent with BTK theory[11] that predicts such an effect only for junctions with $Z < 0.2$ where Z is the dimensionless interface barrier strength.

From BTK theory: $\frac{dI}{dV}(V) \propto \int_{-\infty}^{\infty} \frac{\partial f_0(E-eV)}{\partial(eV)}[1 + A(E) + B(E)]dE$ and $Z = V/\hbar v_F$, the transparency of the S–Sm interfaces can be estimated. Here, $f_0(E)$ is the Fermi Dirac function, $A(E)$ and $B(E)$ are energy dependent Andreev and normal reflection

coefficients respectively. $A(E)$ and $B(E)$ are both Δ_{Nb} and Z dependent. At low temperature and for highly transparent interfaces (transmission $T = 1$ or barrier strength $Z = 0$), all incident electrons undergo Andreev reflection. This results in a reduction of differential resistance within the energy gap. However, if the interface transparency is not good, $T^{-1} = (1 + Z^2) < 1$, part of the incident electrons are normal reflected and there will be competition between the Andreev and normal reflections which results in the increase of the resistance and formation of a zero-bias peak within the gap. This implies that there is a tunneling barrier formed at the S–Sm interfaces. In our experimental results, we did not observe a zero-bias peak in dV/dI (V) curve therefore we can estimate $Z < 0.2$ or $T > 0.96$ for our devices.[6,11] Both the hard gap and SGS are suppressed significantly at temperatures above 400 mK leading to a shift toward zero bias as shown in Figure 3d.

Magnetic Field Dependence of Induced Superconductivity in $In_{0.75}Ga_{0.25}As$: As discussed above we have ballistic junctions with high-transparency superconducting electrodes in contact with a 2DEG where the coherent Andreev reflections and correlation of electrons and holes lead to bound states and therefore phase coherent supercurrents between the electrodes. The color coded plot of dV/dI as a function of applied perpendicular B and applied voltage V is shown in **Figure 4**a at 50 mK. The inset shows dV/dI (V_{SD}) taken at $B_\perp = 2$ mT. The arrows correspond to SGS of $2\Delta/3e$ (cyan), $\Delta/2e$ (green), and $\Delta/3e$ (yellow). We can see that the hard gap and SGS features that are evidence of enhanced multiple Andreev reflections are both suppressed, the position of the peaks shifts toward zero bias and their amplitudes diminishes with further increasing of the applied field. The dV/dI (B)
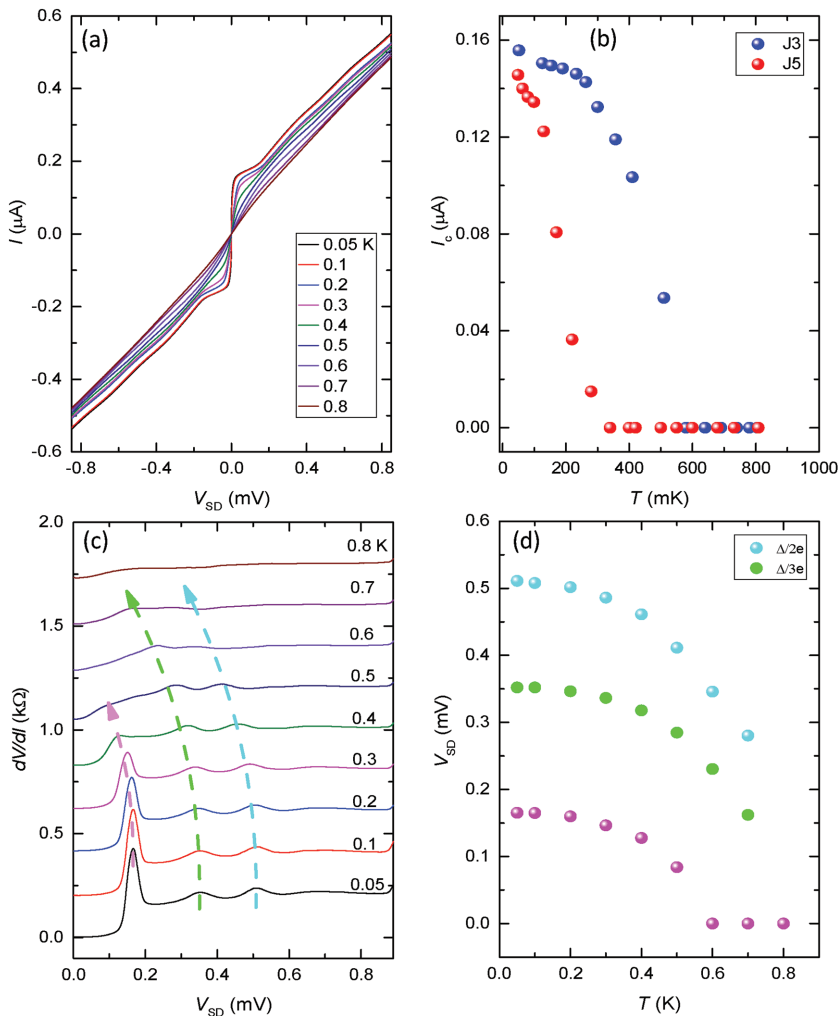
Figure 3. Temperature dependence of induced superconductivity in a ballistic Josephson junction: a) The current–voltage characteristics (IVC) of junction 3. b) Temperature dependence of the critical current I_c as a function of temperature extracted from (a). c) The differential resistance dV/dI as a function of V_{SD} shown in Figure 2b is replotted for positive applied voltages. The cyan, green, and light-pink dashed lines indicate the temperature evolution of the hard- and subharmonic-gap structures. d) The subharmonic-gap structures shift as a function of temperature.

in each junction we have a small area of $A = L \times w = 3.4$ μm^2 with induced superconductivity that is bounded to large areas of ≈ 100 μm^2 in each side of the junction where they are in the normal state. A similar result was also reported in 2DEG (hybrid NbN–GaAs–NbN)[6] as well as nanowire (hybrid Ti/Pb–InAs–Ti/Pb)[18] Josephson junction systems.

To find the amount of flux penetrating the junction area A we should also note the flux crowding.[15,18] This comes from the expelled flux that is pushed into this area due to the screening currents in each Nb electrodes because of the Meissner state in low fields. Figure 4a shows an oscillation of $\Delta B \approx 0.8$ mT which approximately corresponds to an area of $\approx \Delta\Phi/\Delta B \approx 2.5$ μm^2. This is however smaller than the area of the 2DEG between Nb electrodes at closest approach which is ≈ 3.4 μm^2. This does not fit with the expected enhancement of field due to field focusing.[18] The applied magnetic field here is far from the critical filed of Nb so the system is expected to be in full Meissner regime. The following reasons may explain this deviation: i) dephasing from the normal 2DEG regions either side of the junction which reduces the junction's area considerably, and ii) a small amount of static magnetic disorder, and in the 2DEG there is a region formed that acts as quantum dots with an odd number of electrons.[9]

Figure 4b shows the zero-bias differential resistance as a function of the applied parallel and perpendicular magnetic fields. It has been found that in order to get an S–Sm device into a topological regime the condition $g\mu_B B > \Delta_{ind}$ should be satisfied[19] when the main superconductor sustains its gap. Here, g is the Lande g factor and μ_B is the Bohr magneton. We can extract the critical field $B_c^* \approx 500$ mT from Figure 4b where the induced gap in the In$_{0.75}$Ga$_{0.25}$As 2DEG is totally suppressed for both field directions. This critical field is significantly smaller than the critical field of the Nb superconductor ≈ 3 T. If we assume that B_c^* is due to the Zeeman energy surpassing the induced superconductivity gap, i.e., $g\mu_B B = \Delta_{ind}$, our system with $\Delta_{ind} \approx 100$ μeV will have a g-factor ≈ 3.4. This is consistent with the earlier report[20] and the recent experimental measurements of the g-factor in In$_{0.75}$Ga$_{0.25}$As based devices.[21] Our results together with the large g-factor and Rashba spin–orbit coupling in In$_{0.75}$Ga$_{0.25}$As quantum wells, which indeed can be varied by the indium composition, suggest that the Nb–2DEG–Nb system could be an excellent candidate to realize hybrid topological superconducting devices and to possible detection of Majorana modes. Detection of Majorana modes however in a 2D systems is not straightforward as it needs the careful imaging of magnetic vortices' cores or other topological defects
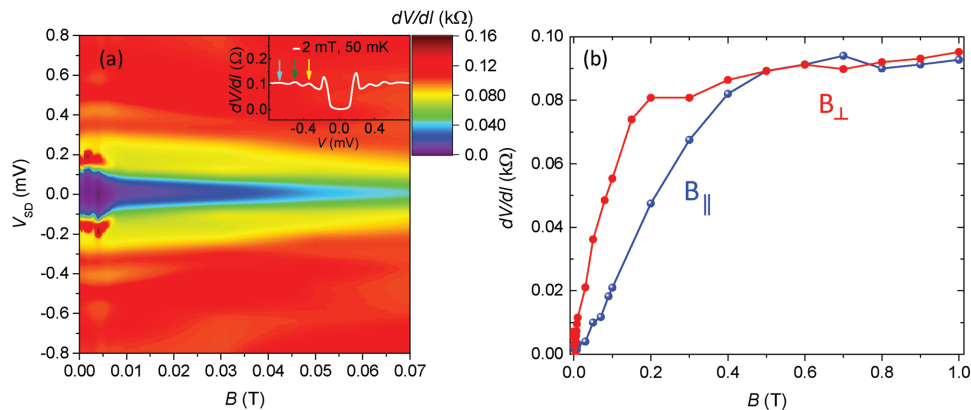
shows Fraunhofer-like oscillation of I_c as seen in Figure 4a for an area of small field between $0 < B_\perp$ (mT) < 1, when no vortices penetrate the superconductor films. This happens as the applied perpendicular field swings the phase of the induced superconductivity in the 2DEG that was confined between Nb superconducting electrodes. The oscillation period of I_c (B) changes continuously and nonmonotonically from Φ_0 to $2\Phi_0$ depending on the size and topology of the devices where $\Phi_0 = h/2e$ is the flux quantum.[14–17] In our device the oscillation of I_c (B) slightly differs from the Fraunhofer pattern that shows a maximum in the supercurrent at zero applied-field and its oscillatory amplitude decays to zero by increasing the field. This is because we have a junction with a length of 850 nm at the shortest path (where the supercurrent is likely to observe) that increases to 26 μm at the end of the active region (where it is unlikely to observe the phase coherent quantum transport). Therefore,

**ADVANCED
SCIENCE NEWS**

www.advancedsciencenews.com

**ADVANCED
MATERIALS**

www.advmat.de

Figure 4. Magnetic field dependence of induced superconductivity in a ballistic Josephson junction: a) Color-coded differential resistance dV/dI as a function of V_{SD} and B at temperature 50 mK. Inset is the dV/dI (B) at 2 mT and measured at 50 mK. Arrows correspond to the SGS. b) The dV/dI versus applied perpendicular (B) and parallel (B) magnetic fields.

in the device which could be located anywhere.[22] Design and fabrication of gated Nb–$In_{0.75}Ga_{0.25}As$–Nb junctions and formation of 1D systems may help to facilitate the detection of these modes in our devices. In S–Sm devices containing gated 1D channels, the g-factor in $In_{0.75}Ga_{0.25}As$ can be increased from ≈3.6 for wide wires (nearly 2D) to >6 for narrow wires[20] so would allow lower B-field observation of Majorana modes. Further development of such devices, i.e., scaling the number of junctions up to 256,[23] provides the possibility for realizing real quantum devices applicable for quantum technology.

We have experimentally demonstrated the successful fabrication of several symmetric, planar, and ballistic Josephson junctions on a chip and performed cryogenic measurements of these devices as a function of temperature and magnetic field. We have shown that proximity induced superconductivity in the $In_{0.75}Ga_{0.25}As$ quantum well 2DEG results in detection of a hard gap and SGS on dV/dI (V_{SD}) characteristics of four out of seven junctions on a chip with critical current values of up to 0.2 µA. We could experimentally prove the formation of highly transparent interfaces between Nb and a 2DEG in an InGaAs wafer with an Andreev transmission probability of >0.96. Our result opens a new road toward hybrid topological quantum systems and helps pave the way for the development of on-chip Andreev devices for realizing the next generation of quantum processors.

Experimental Section

The $In_{0.75}Ga_{0.25}As/In_{0.75}Al_{0.25}As/GaAs$ quantum wells[7] used in this study were grown by MBE. The wafer as shown in Figure 1a from the bottom to the surface comprises a 500 µm GaAs substrate, 50, 75, and 250 nm buffer layers of GaAs, AlAs, and GaAs, a 1300 nm InAlAs step-graded buffer layer, a 250 nm InAlAs buffer layer, a 30 nm 2DEG consisting of an $In_{0.75}Ga_{0.25}As$ quantum well with electron density $n_s = 2.24 \times 10^{11}$ (cm^{-2}) and mobility $\mu_e = 2.5 \times 10^5$ (cm^2 V^{-1} s^{-1}) in the dark and $n_s = 2.28 \times 10^{11}$ (cm^{-2}) and $\mu_e = 2.58 \times 10^5$ (cm^2 V^{-1} s^{-1}) after illumination. The 2DEG quantum well is covered by a 60 nm $In_{0.75}Al_{0.25}As$ spacer, 15 nm of n-type modulation doped $In_{0.75}Al_{0.25}As$, and a 45 nm $In_{0.75}Al_{0.25}As$ layer followed by a 2 nm InGaAs cap layer.[7] Using photolithography and wet etching, in which a sulfuric acid solution of compositions H_2SO_4, H_2O_2, and H_2O was used, we created an active region (a raised area referred to as mesa structure) with length $l' = 1440$

and $w' = 160$ µm in the middle of our chip where all the eight identical junctions are patterned and fabricated (see Figure 1b).

To make junctions, after photolithography patterning we removed the top InGaAs and InAlAs layers in the patterned area using wet etching. The etch produces a 120–140 nm deep trench in this area which is the depth of the $In_{0.75}Ga_{0.25}As$ quantum well. This was followed by deposition of a ≈130 nm Nb film (about three times larger than the London penetration depth of Nb, 40 nm) to make high-quality superconducting contacts to the 2DEG, using DC magnetron sputtering in an Ar plasma. The sample was kept at 50 °C during this process. According to the design, each junction has a length of $L = 850$ nm at the shortest path which increases to 26 µm at the edge of the active region and a width of $w = 4$ µm as shown in Figure 1c. The ohmic contacts were made of gold/germanium/nickel (AuGeNi) to get a low resistance and good chemical bond (adhesion) to the semiconductor substrate and placed 100 µm away from the S–Sm interface to reduce any influence of the normal electrons on the S–Sm interface. Not all of the ohmic pads were used for source–drain bias measurements in this study. Gold wire of diameter 20 µm was used for the bond wires. The quantum transport measurements were performed by using a standard lock-in technique by superimposing a small ac-signal at a frequency of 70 Hz and an amplitude of 5 µV to the junction dc bias voltage and measuring the ac-current.

Conflict of Interest

The authors declare no conflict of interest.

1701836 (5 of 6)

[1] A. F. Andreev, *Sov. Phys. JETP* **1964**, *19*, 1228.

[2] V. Mourik, K. Zuo, S. M. Frolov, S. R. Plissard, E. P. A. M. Bakkers, L. P. Kouwenhoven, *Science* **2012**, *336*, 1003.

[3] L. P. Rokhinson, X. Liu, J. K. Furdyna, *Nat. Phys.* **2012**, *8*, 795.

[4] M. T. Deng, S. Vaitiekėnas, E. B. Hansen, J. Danon, M. Leijnse, K. Flensberg, J. Nygård, P. Krogstrup, C. M. Marcus, *Science* **2016**, *354*, 1557.

[5] W. Chang, S. M. Albrecht, T. S. Jespersen, F. Kuemmeth, P. Krogstrup, J. Nygard, C. M. Marcus, *Nat. Nanotechnol.* **2014**, *10*, 1038.

[6] Z. Wan, A. Kazakov, M. J. Manfra, L. N. Pfeiffer, K. W. West, L. P. Rokhinson, *Nat. Commun.* **2015**, *6*, 7426.

[7] C. Chen, I. Farrer, S. N. Holmes, F. Sfigakis, M. P. Fletcher, H. E. Beere, D. A. Ritchie, *J. Cryst. Growth* **2015**, *425*, 70.

[8] K. Flensberg, J. B. Hansen, M. Octavio, *Phys. Rev. B* **1988**, *38*, 8707.

[9] S. Takei, B. M. Fregoso, H. Hui, A. M. Lobos, S. Das Sarma, *Phys. Rev. Lett.* **2013**, *110*, 186803.

[10] T. D. Stanescu, R. M. Lutchyn, S. Das Sarma, *Phys. Rev. B* **2014**, *90*, 085302.

[11] G. E. Blonder, M. Tinkham, T. M. Klapwijk, *Phys. Rev. B* **1982**, *25*, 4515.

[12] H. Y. Günel, N. Borgwardt, I. E. Batov, H. Hardtdegen, K. Sladek, G. Panaitov, D. Grützmacher, Th. Schäpers, *Nano Lett.* **2014**, *14*, 4977.

[13] J. C. Cuevas, J. Hammer, J. Kopu, J. K. Viljas, M. Eschrig, *Phys. Rev. B* **2006**, *73*, 184505.

[14] I. K. Marmorkos, C. W. J. Beenakker, *Phys. Rev. B* **1993**, *48*, 4.

[15] J. P. Heida, B. J. van Wees, J. J. Kuipers, T. M. Klapwijk, G. Borghs, *Phys. Rev. B* **1998**, *57*, 11911.

[16] J. C. Cuevas, F. S. Bergeret, *Phys. Rev. Lett.* **2007**, *99*, 217002.

[17] V. Barzykin, A. M. Zagoskin, *Superlattices Microstruct.* **1999**, *25*, 797.

[18] J. Paajaste, M. Amado, S. Roddaro, F. S. Bergeret, D. Ercolani, L. Sorba, F. Giazotto, *Nano Lett.* **2015**, *15*, 1803.

[19] M. Kjaergaard, F. Nichele, H. J. Suominen, M. P. Nowak, M. Wimmer, A. R. Akhmerov, J. A. Folk, K. Flensberg, J. Shabani, C. J. Palmstrøm, C. M. Marcus. *Nat. Commun.* **2016**, *7*, 12841.

[20] T. P. Martin, A. Szorkovszky, A. P. Micolich, A. R. Hamilton, C. A. Marlow, H. Linke, R. P. Taylor, L. Samuelson, *Appl. Phys. Lett.* **2008**, *93*, 012105.

[21] Y. Gul, G. L. Creeth, D. English, S. N. Holmes, K. J. Thomas, I. Farrer, D. J. Ellis, D. A. Ritchie, M. Pepper, unpublished.

[22] M. Franz, *Nat. Nanotechnol.* **2013**, *8*, 149.

[23] H. Al-Taie, L. W. Smith, B. Xu, P. See, J. P. Griffiths, H. E. Beere, G. A. C. Jones, D. A. Ritchie, M. J. Kelly, C. G. Smith, *Appl. Phys. Lett.* **2013**, *102*, 243102.

1701836 (6 of 6)